Fine-Scale Nanostructure in γ-Al₂O₃

Gianluca Paglia, Emil S. Božin, and Simon J. L. Billinge*

Biomedical Physical Sciences, Department of Physics and Astronomy, Michigan State University, East Lansing, Michigan 48824-2320
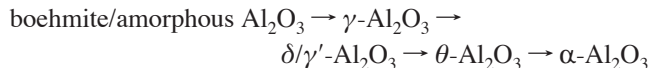
We have applied a local structural technique, atomic pair distribution function (PDF) analysis of powder diffraction data to γ-Al₂O₃, to obtain a quantitative structure. Refinements of the PDF support previous findings that nonspinel model representations are more suitable to describe the average structure of γ-Al₂O₃, as opposed to the spinel model. Surprisingly, also we find a previously unknown fine-scale nanostructure with a domain size ∼ 1 nm. Modeling suggests that within these nanodomains the oxygen sublattice is modified from the average structure and retains aspects of the boehmite precursor that reflects a stacking fault in the γ-Al₂O₃ matrix. This results in a novel and unexpected view of the γ-Al₂O₃ structure because earlier controversies about it centered on the arrangement of Al ions among different cation sites, whereas the oxygen sublattice arrangement was rarely questioned. This average oxygen sublattice structure is recovered in our models on longer length scales by introducing aperiodic arrays of stacking faults. The use of γ-Al₂O₃ in catalysis depends sensitively on its nanoporosity and defect structure. Here we present a new view which may allow for additional understanding and optimization of its functional properties.

Introduction

Of the many stable phases of alumina,[1] the γ phase is one of the most important with numerous applications such as in catalysts and catalytic supports.[2–7] Despite its industrial importance, details of the structure remain unresolved largely as a result of the 15–30 nm domain nanocrystalline nature[8] of γ-Al₂O₃ that makes single-crystal structure solution impossible. Structural characterization has been carried out using electron diffraction and X-ray and neutron powder diffraction, where the peaks are found to be broad and diffuse.[9–19]

γ-Alumina is reported to occur at temperatures between 350 and 1000 °C.[9,20] It is typically formed from an amorphous or boehmite precursor and has remained present at temperatures as high as 1200 °C when derived from amorphous aluminas.[21] It occurs in the following transformation sequence:

$$\text{boehmite/amorphous Al}_2\text{O}_3 \rightarrow \gamma\text{-Al}_2\text{O}_3 \rightarrow$$
$$\delta/\gamma'\text{-Al}_2\text{O}_3 \rightarrow \theta\text{-Al}_2\text{O}_3 \rightarrow \alpha\text{-Al}_2\text{O}_3$$

Traditionally the structure was thought of as a cubic spinel,[14–16,22,23] with some suggestion of a tetragonal distortion in boehmite-derived γ-Al₂O₃,[9,10,12,13] in the I4₁/amd space group.[17,24] However, the cubic and tetragonally distorted spinel models yield poor fits to the powder data due to the appearance of extra peaks in the calculated patterns.[17] It has been suggested that improved fits are possible when hydrogen is introduced into the bulk crystalline matrix.[25] The presence of hydrogen in the samples is supported by other studies,[26,27] though its existence in the bulk crystalline matrix

---

* Correspondence and requests for materials should be addressed to Prof. Simon Billinge. E-mail: billinge@pa.msu.edu.
(1) Wefers, K.; Misra, C. *Oxides and Hydroxides of Aluminum*; Technical Paper No. 19 Alcoa Laboratories: Pittsburgh, 1987.
(2) Satterfield, C. N. *Heterogeneous Catalysis in Practice*; McGraw-Hill: New York, 1980.
(3) Knözinger, H.; Ratnasamy, P. *Catal. Rev.–Sci. Eng.* **1978,** *17,* 31–70.
(4) Xu, Z.; Xiao, F. S.; Purnell, S. K.; Alexeev, O.; Kawi, S.; Deutsch, S. E.; Gates, B. C. *Nature* **1994,** *372,* 346–348.
(5) Gates, B. C. *Chem. Rev.* **1995,** *95,* 511–522.
(6) Maillet, T.; Barbier, J., Jr.; Gelin, P.; Praliaud, H.; Duprez, D. *J. Catal.* **2001,** *202,* 367–378.
(7) Prins, R. *Adv. Catal.* **2001,** *46,* 399–464.
(8) Paglia, G.; Buckley, C. E.; Rohl, A. L.; Winter, K.; Hart, R. D.; Hunter, B. A.; Studer, A.; Hanna, J. V. *Chem. Mater.* **2004,** *16,* 220–236.
(9) Lippens, B. C.; de Boer, J. H. *Acta Crystallogr.* **1964,** *17,* 1312–1321.
(10) Yanagida, H.; Yamaguchi, G. *Bull. Chem. Soc. Jpn.* **1964,** *37,* 1229–1231.
(11) Saalfeld, H.; Mehrotra, B. *Ber. Dtsch. Keram. Ges.* **1965,** *42,* 161–165.
(12) Wilson, S. J. *J. Solid State Chem.* **1979,** *30,* 247–255.
(13) Wilson, S. J.; McConnell, J. D. C. *J. Solid State Chem.* **1980,** *34,* 315–322.
(14) Zhou, R. S.; Snyder, R. L. *Acta Crystallogr., Sect. B* **1991,** *47,* 617–630.
(15) Wang, Y. G.; Bronsveld, P. M.; DeHosson, J. T. M. *J. Am. Ceram. Soc.* **1998,** *81,* 1655–1660.
(16) Wang, J. A.; Bokhimi, X.; Morales, A.; Novaro, O.; Lopez, T.; Gomez, R. *J. Phys. Chem. B* **1999,** *103,* 299–303.
(17) Paglia, G.; Buckley, C. E.; Rohl, A. L.; Hunter, B. A.; Hart, R. D.; Hanna, J. V.; Byrne, L. T. *Phys. Rev. B* **2003,** *68,* 144110.
(18) Paglia, G.; Rohl, A. L.; Buckley, C. E.; Gale, J. D. *Phys. Rev. B* **2005,** *71,* 224115.
(19) Paglia, G.; Buckley, C. E.; Udovic, T. J.; Rohl, A. L.; Jones, F.; Maitland, C. F.; Connolly, J. *Chem. Mater.* **2004,** *16,* 1914–1923.
(20) O'Connor, B. H.; Li, D.; Gan, B. K.; Latella, B.; Carter, J. *Adv. X-Ray Anal.* **1997,** *41,* 659–667.
(21) Tung, S. E.; Mcininch, E. J. *Catal.* **1964,** *3,* 229–238.
(22) Ernst, F.; Pirouz, P.; Heuer, A. H. *Philos. Mag. A* **1991,** *63,* 259–277.
(23) Wolverton, C.; Hass, K. C. *Phys. Rev. B* **2001,** *63,* 024102.
(24) Li, D. Y.; O'Connor, B. H.; Roach, G. I. D.; Cornell, J. B. *XVth Congress of the International Union of Crystallography (Bordeaux)*; 1990, (Abstracts Vol. C-61).
(25) Ushakov, V. A.; Moroz, E. M. *React. Kinet. Catal. Lett.* **1984,** *24,* 113–118.
(26) Tsyganenko, A. A.; Mirnov, K. S. S.; Rzhevskij, A. M.; Mardilovich, P. P. *Mater. Chem. Phys.* **1990,** *26,* 35–46.

γ-Al₂O₃ Fine-Scale Nanostructure

Chem. Mater., Vol. 18, No. 14, 2006 3243

has been determined to be unlikely in recent studies.[14,17,19,23] In these latter studies, an attempt was made to fit models containing deuterium to deuterated γ-Al$_2$O$_3$ neutron diffraction data and found that the best fits were obtainable with anhydrous (non-hydrogenated) models.[17] Alternatively, improved fits to the diffraction data were possible when some nonspinel sites are allowed to be occupied by cations in the absence of hydrogen.[14] The spinel cation sites are Wyckoff *a* and *d* sites (octahedral and tetrahedral sites, respectively). An earlier suggestion that partial occupancy by Al of the octahedral *e* site, at the expense of the *d* site, gave better fits.[14] More recent investigations found it more appropriate to have partial occupancy of the Wyckoff *c* site, which also gives a quantitatively good Rietveld fit[8,17] and is preferred on energetic grounds on the basis of interatomic potential and density functional theory (DFT) calculations.[18,23,28] Furthermore, following from the results of refs 8, 17, and 19, ref 18 also shows, after an exhaustive computational study whereby simulated diffraction patterns of the modeled structures were compared to experiment, that nonspinel occupancy is required to achieve a diffracton pattern that closely matches that of experiment.[29] This was also supported by the theoretical study of Menendez-Proupin and Gutierrez.[30] We set out to test these models (spinel and *c* symmetry based nonspinel)[17,18] against atomic pair distribution function (PDF)[31] data, a method that has shown itself to yield useful structural information from disordered materials such as γ-Al$_2$O$_3$.[31–34]

The atomic PDF is defined as

$$G(r) = 4\pi r[\rho(r) - \rho_0] \qquad (1)$$

where $\rho(r)$ is the atomic pair density, ρ_0 is the average atomic number density, and r is the radial distance.[35] The PDF is a measure of the probability of finding pairs of atoms separated by a distance r. It is obtained by a sine Fourier transformation

(27) Sohlberg, K.; Pennycook, S. J.; Pantelides, S. T. *J. Am. Ceram. Soc.* **1999**, *121*, 7493–7499.

(28) Krokidis, X.; Raybaud, P.; Gobichon, A.-E.; Rebours, B.; Euzen, P.; Toulhoat, H. *J. Phys. Chem. B.* **2001**, *105*, 5121–5130.

(29) Another study, using DFT and models fitted by Rietveld analysis to XRD data, by Sun et al. (*J. Phys. Chem. B* **2006**, *110*, 2310–2317), concluded that the 'spinel related model is better than the nonspinel model in description of the bulk structure of γ-Al$_2$O$_3$.' This finding was based on the comparison of 12 hydrogenated and non-hydrogenated spinel structural models to a solitary nonspinel model, that presented by Digne et al. (*J. Catal.* **2004**, *226*, 54–68). However, Sun et al. paper did not account for the findings of the Paglia et al. series of studies, in particular, ref 17, where a larger array of structural possibilities were examined using neutron diffraction data of deuterated γ-Al$_2$O$_3$ (as opposed to X-ray scattering data which cannot "see" hydrogen). This included spinel, nonspinel (that introduced in the ground breaking Zhou and Snyder study (ref 14) and those models introduced in ref 17 itself), cubic (spinel and nonspinel), tetragonal (spinel and nonspinel), dual phase, and hydrogenated models (spinel, nonspinel, cubic, tetragonal, and using two different stoichiometric approaches). The main finding of the Paglia et al. series of studies is, as can be seen in the introduction here, opposite to that of Sun et al.

(30) Menendez-Proupin, E.; Gutierrez, G. *Phys. Rev. B* **2005**, *72*, 035116.

(31) Egami, T.; Billinge, S. J. L. *Underneath the Bragg Peaks – Structural Analysis of Complex Materials*; Pergamon: Oxford, 2003.

(32) Billinge, S. J. L.; Kanatzidis, M. G. *Chem. Commun.* **2004**, 749–760.

(33) Petkov, V.; Billinge, S. J. L.; Larson, P.; Mahanti, S. D.; Vogt, T.; Rangan, K. K.; Kanatzidis, M. G. *Phys. Rev. B* **2002**, *65*, 092105.

(34) Gilbert, B.; Huang, F.; Zhang, H.; Waychunas, G. A.; Banfield, J. F. *Science* **2004**, *305*, 651–654.

of the reciprocal space total scattering structure function $S(Q)$, obtained from a diffraction experiment. This approach is widely used for studying liquids and amorphous materials but has recently been successfully applied to nanocrystalline materials.[32] The advantage of using this technique over the traditional Bragg diffraction analysis is that it incorporates all components for the diffraction intensities; both Bragg and diffuse scattering contributions are considered equally, which is imperative when accurate structural information about poorly crystalline materials is required. Because the PDF produces quantitative information from materials that scatter diffusely, it is employed here to assess the structure of the γ-Al$_2$O$_3$, using data obtained from the same materials used in previous studies.[17,19]

The models under consideration differ in the arrangement of aluminum cations among possible interstitial sites in the oxygen sublattice. As we discuss below, the *c* symmetry model, where $\approx$43% of the cations are situated on nonspinel positions, performed best in the high-*r* region of the PDF. However, unexpectedly, none of the models could explain the low-*r* region of the PDF suggesting a previously unsuspected 10 Å length-scale structure present in these materials. This could only be fit by modifying the oxygen sublattice. The average oxygen sublattice is recovered from the modified local structure by introducing stacking faults that are aperiodically arranged.

Experimental Methods

The γ-Al$_2$O$_3$ was prepared by calcining highly crystalline boehmite at 600 °C for 7 h.[8] The finely powdered sample was packed and sealed with Kapton tape in flat plates of 1.0 mm thickness. Ambient temperature transmission X-ray scattering experiments were conducted on these samples at the 6-IDD MUCAT beam line at the Advanced Photon Source (APS), Argonne National Laboratory, using an incident energy of 87.005 keV (λ = 0.142 479 Å). The diffraction data were obtained using the recently developed rapid acquisition PDF technique.[36] Data collection was carried out for 4000 s, in 500 s intervals, using an automated Mar345 image plate camera, mounted orthogonal to the beam with a calibrated sample to detector distance of 208.857 mm. Using the program Fit2D,[37] the raw data sets obtained were normalized with respect to the monitor counts and then integrated to produce one-dimensional X-ray diffraction (XRD) data. The normalized XRD pattern obtained for the γ-Al$_2$O$_3$ sample is shown in Figure 1, which also displays the diffraction pattern for the crystalline boehmite precursor for comparison. The boehmite (Figure 1b) exhibited a lower diffuse background and well-defined Bragg peaks up to a high wave vector of $Q > 12$ Å^{-1} ($Q = 4\pi \sin \theta/\lambda$, where θ is the angle of the incident radiation and λ is the wavelength). By comparison, the γ-Al$_2$O$_3$ sample contains fewer Bragg-like features and a considerably larger diffuse component. This is particularly evident when viewing the inset of Figure 1a which shows the high-*Q* data on the same expanded scale as the inset in Figure 1b. Diffraction patterns such as those for the γ-Al$_2$O$_3$ are characteristic of materials with nanoscale order.[32]

(35) Warren, B. E. *X-ray Diffraction*; Dover: New York, 1990.

(36) Chupas, P. J.; Qiu, X.; Hanson, J. C.; Lee, P. L.; Grey, C. P.; Billinge, S. J. L. *J. Appl. Crystallogr.* **2003**, *36*, 1342–1347.
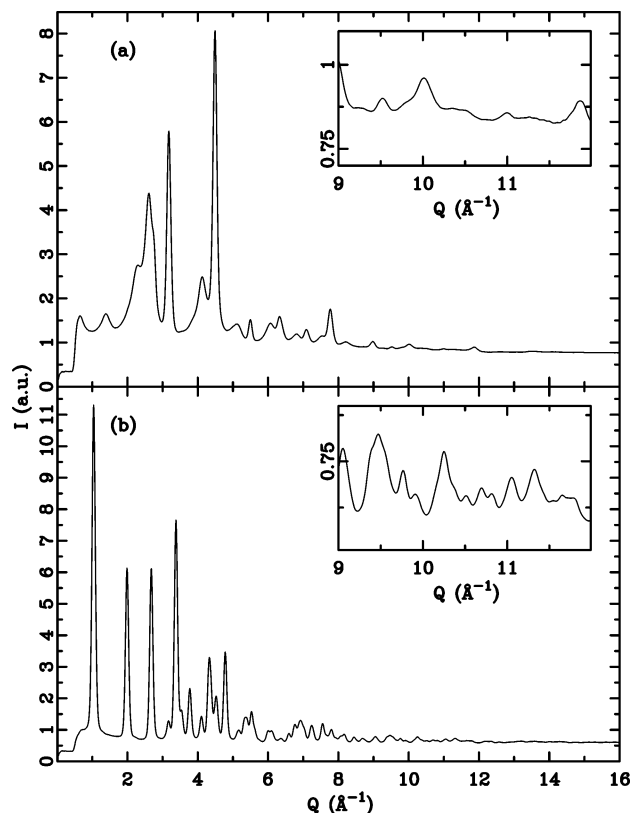
3244   *Chem. Mater., Vol. 18, No. 14, 2006*

Paglia et al.

Figure 1. Experimental powder diffraction patterns for (a) γ-Al_2O_3 and (b) the crystalline boehmite precursor shown for comparison. The insets show amplified $I(Q)$ data at high Q.

Figure 2. Experimental reduced structure functions, $F(Q)$, for (a) γ-Al_2O_3 and (b) the crystalline boehmite precursor shown for comparison.

Conversion of the XRD data to the scattering functions and PDFs was performed using PDFgetX2.[38] The reduced structure functions, $F(Q)$, were truncated at Q_{max} of 20 Å^{-1} before the PDF was calculated. The reduced structure functions and PDFs obtained are shown in Figures 2 and 3, respectively. The peaks in the PDF data below 1.5 Å are unphysical and can be neglected. They originate from unavoidable systematic errors in the data arising from noise at high Q and termination effects due to the finite Q_{max} used. They are shown for the purpose of gauging the quality of the PDF and can be seen to largely die out to the level of the noise before the first physical peak (Al–O) at 1.85 Å. Comparison between the data in Figures 1–3 illustrates why this approach yields quantitative local structural information in nanostructured materials. First, the data-reduction step to obtain $F(Q)$ results in an amplification of the important diffuse signal at high Q, which provides critically important information about the local structure. This is somewhat neglected in the XRD pattern of γ-Al_2O_3 (Figure 1a), which is dominated by strong Bragg peaks at low Q, and illustrates how conventional XRD analysis is predominantly sensitive to long-range order.

The resulting PDFs from nanostructured materials are often sharp, well-defined functions in real space, and the enhanced sensitivity to the local atomic ordering in the PDF makes it well-suited for the structure determination of materials with limited structural coherence.

Once the PDF is obtained, an approach similar to Rietveld analysis[39] can be followed.[40] The least-squares PDF-profile fitting
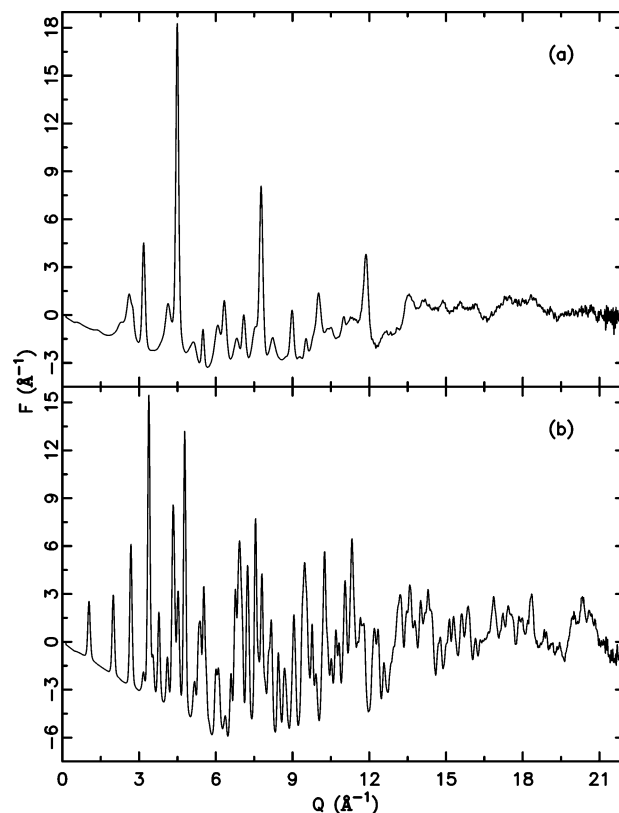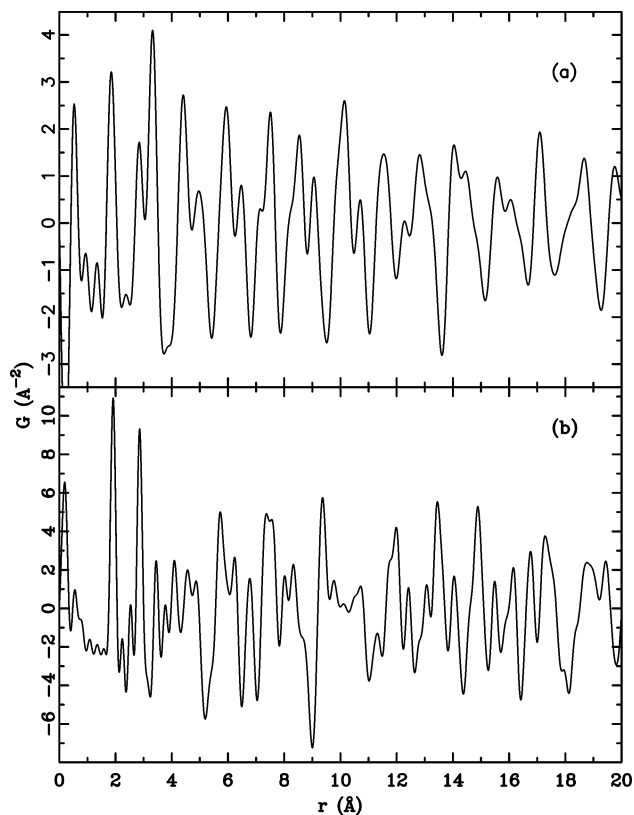

Figure 3. Experimental PDFs for (a) γ-Al_2O_3 and (b) the highly crystalline boehmite precursor, obtained by Fourier transforming the data in Figure 2.

program PDFFIT[41] was used to perform refinements of the structural models to the PDF. The effectiveness of this method of solving the structures of disordered materials has been demonstrated previously.[32,42]
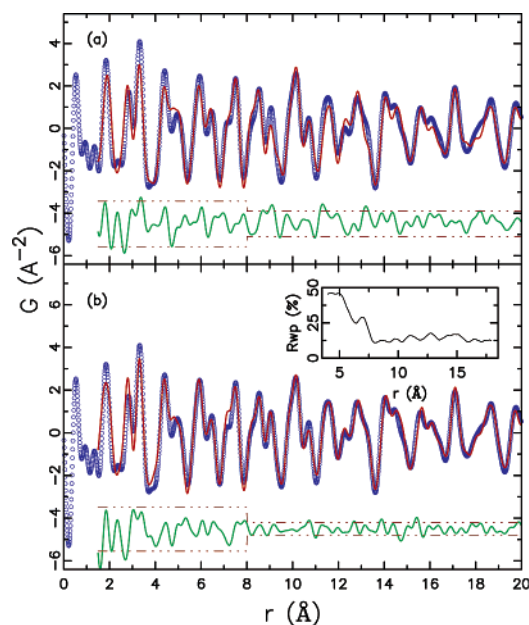
(37) Hammersley, A. P.; Svenson, S. O.; Hanfland, M.; Hauserman, D. *High Pressure Res.* **1996**, *14*, 235−248.
(38) Qiu, X.; Thompson, J. W.; Billinge, S. J. L. *J. Appl. Crystallogr.* **2004**, *37*, 678.
(39) Rietveld, H. M. *J. Appl. Crystallogr.* **1969**, *2*, 65−71.

γ-Al₂O₃ Fine-Scale Nanostructure

Chem. Mater., Vol. 18, No. 14, 2006 3245

Figure 4. Comparison between the experimental PDF for γ-Al$_2$O$_3$ (symbols) and the calculated PDF (solid line) for (a) the spinel model (R_{wp} = 32.7% for the total fit and 29.1% for 8 Å $< r <$ 20 Å) and (b) the c symmetry-based nonspinel model derived from molecular modeling[18] (R_{wp} = 27.5% for the total fit and 15.8% for 8 Å $< r <$ 20 Å). The solid line, offset below each PDF, shows the difference between the experimental and calculated PDFs. The dashed line bordering the difference curves represents the 2σ standard deviation of all the points in the curves for the regions below and above r = 8 Å. An inset is shown for the c symmetry-based nonspinel model fit illustrating the variation in R_{wp} over the range of the PDF, emphasizing the sharp increase below 8 Å. See text for details.

Results and Discussion

The two candidate models that were initially fit to the PDF are the traditional spinel-based model and the recently determined c symmetry-based model derived from molecular modeling.[18] These models were refined both in their $26\frac{2}{3}$ atom single unit cell form, a virtual crystal with partial occupancy on some cation sites, and as a $2 \times 1 \times 3$ supercell to yield an integral number of atoms.[18] Only models that were described under the tetragonal $I4_1/amd$ space group were used here as it is known that the material being examined is the tetragonally distorted form of γ-Al$_2$O$_3$.[17] The starting structures of the models were taken directly from refs 17 and 18 and are fully relaxed structures within the DFT, generalized gradient approximation. Initially the atomic coordinates were held fixed, and only lattice parameters and thermal factors were allowed to vary in the refinement. The results are shown in Figure 4. The c symmetry-based nonspinel model has a lower weighted agreement factor, R_{wp}, and smaller fluctuations in the residuals curve than does the spinel model suggesting that it gives the better description of the structure. However, it is apparent that neither model fits the data well below 8 Å. Accordingly, the atomic coordinates in both models were allowed to vary in the refinement for a total of 9 and 12 parameters, as allowed by symmetry, in the spinel and c symmetry models, respectively. However, this did not improve the quality of the fits in the

Table 1. Refined Parameters for the γ-Al$_2$O$_3$ Local Structure Model for 1.4 Å $< r <$ 8 Å.^{a}

atom	$a = 3.4009(6)$ Å, $b = 2.7895(3)$ Å, $c = 7.0762(9)$ Å			
	x	y	z	U (Å^2)
O	0.7867(2)	0.5598(1)	0.0785(3)	0.0007(1)
O	0.2418(3)	0.9879(2)	0.2493(2)	0.0069(1)
O	0.7791(1)	0.4825(3)	0.3987(3)	0.0069(1)
O	0.2007(6)	0.4656(2)	0.5901(2)	0.0069(1)
O	0.8282(2)	0.9922(1)	0.7515(4)	0.0069(1)
O	0.2756(3)	0.6089(3)	0.9300(3)	0.0069(1)
Al	0.2091(4)	0.4855(3)	0.0652(3)	0.0110(2)
Al	0.4485(3)	0.9782(1)	0.4620(4)	0.0110(2)
Al	0.2802(2)	0.0307(3)	0.7138(2)	0.0110(2)
Al	0.5934(3)	0.4773(3)	0.8726(3)	0.0110(2)

^{a} All species have occupancies set to 1.00.

low-r region. This was also found to be the case when the models were then allowed to refine under $P1$ symmetry, and all the atom coordinates were eventually relaxed. The model in $P1$ symmetry is highly parametrized, yet still a good solution, given the starting model and the downhill (Levenburg-Marquardt) regression scheme, could not be found suggesting that the local structure ($r < 8$ Å) is significantly different from the starting structures, as we discuss below.

To quantify the r dependence of the fit we evaluated R_{wp} over limited r ranges of the data. In the inset to Figure 4b, we plot $R_{wp}(r)$, which is defined as the value of R_{wp} evaluated over the range $\delta r = 3.9$ Å, centered on the position r. R_{wp}-(r) increases sharply below 8 Å. This behavior is also directly evident from the difference curves of the model fits (Figure 4) where the amplitude of the difference plots clearly increases below 8 Å. The dashed lines above and below the difference curves indicate $2 \times$ the standard deviation of the points in the difference plots for the regions above and below 8 Å (Figure 4). The c symmetry and spinel models provide an equally poor fit to the *local* structure, with R_{wp} = 31.7 and 32.2%, respectively. However, above 8 Å (and up to 20 Å) R_{wp} values of 29.1 and 15.8% were obtained for the spinel and c symmetry models, respectively. The c symmetry-based nonspinel model is clearly preferred for the average structure; however, the *local* structure is modified. Different local and average structures can be reconciled when local domains of lower symmetry are averaged, for example, orientationally, in such a way as to recover a higher symmetry average structure.[42] In this case, the PDF, depending on r, provides both the intra- and interdomain structures and crosses smoothly from the local to the average structure. In the absence of a modified local structure, the local and average structures are the same and there is no crossover.[43] The local structural information originates from the diffuse scattering of the diffraction data. In the case of γ-Al$_2$O$_3$ it is apparent that a different local structure exists in the range 0−1 nm that is not captured by the average models, and the crystal structure is some average of this local structure.

As indicated in previous studies, γ-Al$_2$O$_3$ is comprised of platelike grains which are composed of 15−30 nm lamellar crystallites,[8,19] forming a lamellar porous nanostructure.[12,44]

(40) Billinge, S. J. L. In *Local Structure from Diffraction*; Billinge, S. J. L., Thorpe, M. F., Eds.; Plenum: New York; 1998, p 137.

(41) Proffen, Th.; Billinge, S. J. L. *J. Appl. Crystallogr.* **1999**, *32*, 572−575.

(42) Petkov, V.; Billinge, S. J. L.; Heising, J.; Kanatzidis, M. G. *J. Am. Chem. Soc.* **2000**, *122*, 11571−11576.

(43) Qiu, X.; Proffen, Th.; Mitchell, J. F.; Billinge, S. J. L. *Phys. Rev. Lett.* **2005**, *94*, 177203.
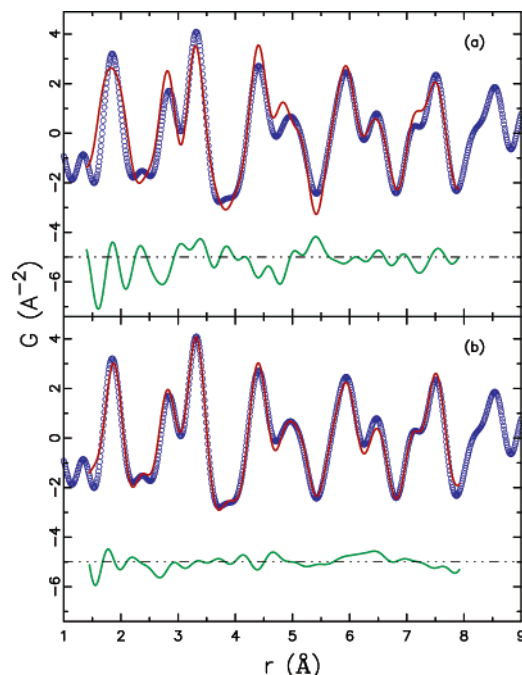
Figure 5. Comparison, for 1.4 Å < r < 8 Å, between the experimental PDF for γ-Al$_2$O$_3$ (symbols) and calculated PDFs (solid lines) for (a) the c symmetry-based nonspinel model derived from molecular modeling,[18] R_{wp} = 31.7%, and (b) the local structure model, R_{wp} = 15.3%. The solid line below each PDF is the difference between the experimental and calculated PDF.

The low-r region of the PDF indicates a modified local structure which exists *within* the confines of the lamellar crystallites. Thus, γ-Al$_2$O$_3$ can be viewed as a multiscale structure, with the 15–30 nm and greater length scales represented by average structural models that provide suitable Rietveld refinements to model Bragg diffraction data, and the newly identified 0–1 nm local structure.

γ-Al$_2$O$_3$ can, theoretically, exhibit a surface area as high as 560 m^2 g^{-1},[45] and it is interesting to consider whether the modified local structure observed in the PDF is reflecting surface modifications.[14] The measured surface area of the γ-Al$_2$O$_3$ sample examined here was 122 m^2 g^{-1}.[19] Given a polygonal crystallite with a maximum length of 30 nm, the percentage number of cations at the surface is estimated to be less than 4%. Such an effect would be barely visible in the PDF, and we conclude that the observed data must reflect a modified local structure in the bulk.

A local structure was then sought that would explain the low-r PDF that could also be rationalized with the observed average structure. Primitive cells of the average structure models were first tried, but the cations and anions were selectively allowed to relax without maintaining the symmetry restrictions. This approach would allow localized distortions of octahedra and tetrahedra that were observed from previous molecular modeling studies.[18] However, these refinements did not result in improved fits when compared to the average structure models, indicating that the modified local structure cannot be explained in this way.

A successful local structure model, whose fit to the low-r region is shown in Figure 5b, was found by considering the transformation of boehmite to γ-Al$_2$O$_3$. The boehmite
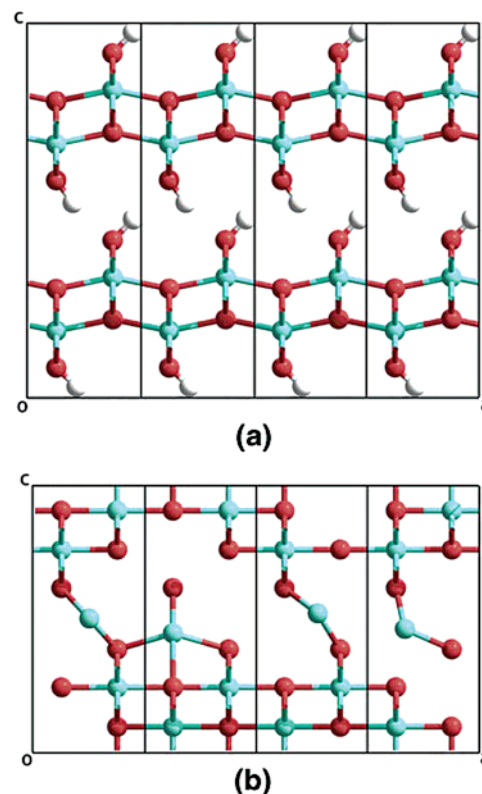
---

(44) Soled, S. *J. Catal.* **1983**, *81*.

Figure 6. Illustration of (a) the boehmite unit cell with a = 3.692 Å, b = 2.868 Å, and c = 12.234 Å[46] and (b) example starting configurations for the local structure model of γ-Al$_2$O$_3$, with a = 3.692 Å, b = 2.868 Å, and c = 7.534 Å. Four unit cells are shown for illustrative purposes. In part b different Al ions have been migrated to illustrate examples of different bridging possibilities in each cell. The bridging atoms result in highly distorted octahedra and tetrahedra, which are not easily observed from the two-dimenional perspective drawn here. These different possibilities prevent the local order from propogating over the long range.

structure consists of alternating double layers of aluminum-containing oxygen layers (the skeletal layers) and hydrogen-containing oxygen layers (Figure 6a).[1] Upon breakdown at ≈400 °C,[1] hydrogen leaves the structure and six Al–O layers remain, forming the skeletal framework that evolves into γ-Al$_2$O$_3$.[9,12] In boehmite all the cations in the skeletal layers are octahedrally coordinated, and the apical O–Al–O angle of each octahedron is approximately 160°.[46] In γ-Al$_2$O$_3$ the apical angle of each octahedron is the ideal 180°. The formation of the γ-Al$_2$O$_3$ structure is assumed to proceed as a short-range migration of cations (Al) into site positions within the interskeletal layers, with the oxygens moving to accommodate the cation migration.[8] The breakdown of the OH layers of boehmite results in the formation of the lamellar porous nanostructure of γ-Al$_2$O$_3$.[12] These pores can contain a poorly ordered "amorphous" alumina content, are hydrogen-containing, and can contain other Al–O species of varying stoichiometries.[19] As the structure of γ-Al$_2$O$_3$ evolves there is a counter-migration of three protons to the surface for each cation that moves into the interskeletal layer regions.[12,47]

---

(45) Wilson, S. J.; Stacey, M. H. *J. Colloid Interface Sci.* **1981**, *82*, 507–517.
(46) Corbato, C. E.; Tettenhorst, R. T.; Christoph, G. G. *Clays Clay Miner.* **1985**, *33*, 71–75.
(47) Tsuchida, T.; Furuichi, R.; Ishii, T. *Thermochim. Acta* **1980**, *39*, 103–115.

γ-Al₂O₃ Fine-Scale Nanostructure

Chem. Mater., Vol. 18, No. 14, 2006   3247

Table 2. Idealized Coordinates for the Local Structure Model Described under *Pmma* Space Group Symmetry

atom	x	y	z	occupancy
O(2e)	0.25	0.0	0.2500	1.000
O(2f)	0.25	0.5	0.1000	1.000
O(2f)	0.25	0.5	0.3800	1.000
Al(2c)	0.0	0.0	0.5	0.
Al(2e)	0.25	0.0	0.7500	0.333
Al(2e)	0.25	0.0	0.2500	0.333
Al(2f)	0.25	0.5	0.1000	0.333
Al(4i)	0.5	0.5	0.2500	0.333

Table 1 contains the structural parameters for the local model refined under $P1$ symmetry. We propose that an idealized description of the model can be provided under *Pmma* space group symmetry (Table 2). The total number of structural parameters refined for the local model was 15, slightly more than for the average models, which had a maximum of 12 parameters. This indicates that the local model was not over parametrized. The fit of the local model was superior in the low-r range, 1.4 Å $< r <$ 8 Å, compared with the average model (R_{wp} = 15.3 compared to R_{wp} = 31.7%). The structural parameters for the average model used in this comparison were taken from refs 17 and 18.

The local structural model presented here essentially represents the bridging of the skeletal layers that form the unit cell of γ-Al₂O₃. The starting configuration for this was obtained by modifying the unit cell of boehmite to reflect the description above. All hydrogens and two oxygens were removed from the cell such that only four aluminums and six oxygens remain, maintaining the correct 2:3 stoichiometry. Cations and anions were aligned in the c direction to produce the ideal 180° apical O–Al–O angle expected for γ-Al₂O₃. Finally, one cation was moved into a tetrahedrally or octahedrally coordinated position around the center of the cell to represent the bridging of the skeletal layers of the unit cell (Figure 6b). These bridging atoms result in highly distorted octahedra and tetrahedra linking the two halves of the local model. This unit cell (Table 1) with 10 atoms is considerably smaller than the average tetragonal $I4_1/amd$ structural model[17] that has $26^{2}/_{3}$ atoms. The c axis of the local model is parallel to the c axis in the average tetragonal model. The key aspect is that the structural relationship between γ-Al₂O₃ and its boehmite precursor results in an oxygen sublattice that is locally faulted with respect to the average structure of γ-Al₂O₃, as we describe below.

Several versions of the model were attempted with cations in different bridging site positions, each resulting in an adequate fit to the data. The best fit of the local structure model to the low-r region of less than 8 Å is illustrated in Figure 5b. The local model also exhibited smaller thermal factors than the average models refined over the same range, lending confidence that it is a correct description of the local structure. The cations displayed larger thermal parameters than the oxygens, which maybe is not surprising as these species undergo continual migration during the topotactic boehmite to θ-Al₂O₃ phase transition sequence.[8,9,12] The local structural model therefore provides a snapshot of the continuous localized ordering processes that occur during this phase transition sequence.

We now discuss the nature of the stacking fault of the oxygen sublattice that reconciles the local and average
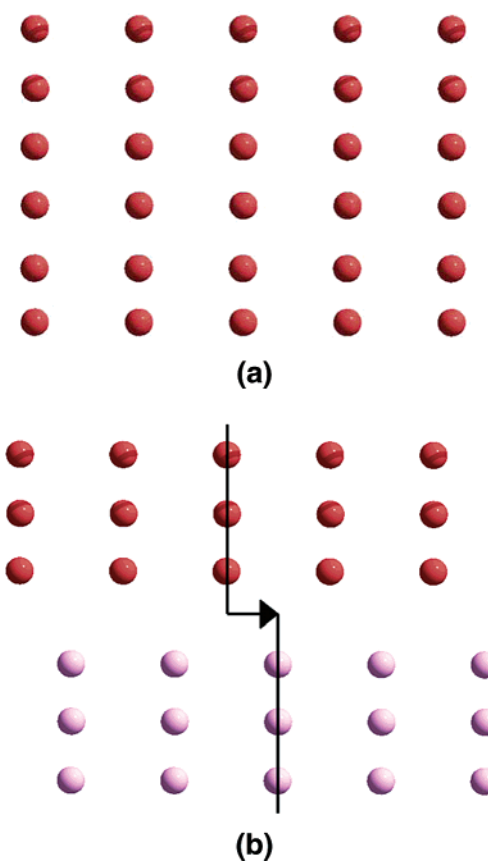

Figure 7. Illustration of the oxygen sublattice viewed down the tetragonal (2̄20) planes for (a) the average model and (b) the nanomodel which illustrates the relative displacement of the two domains by approximately 1.8 Å in the [220] direction. The two different colors represent the two offset groups of oxygen atoms. Two lines have been drawn in the faulted oxygen sublattice connected by an arrow to further highlight the shift. Aluminum has not been included for clarity.

structural models. The plane of the stacking fault is (002) resulting from a relative displacement of the oxygen sublattice of approximately 1.8 Å in the [220] direction (Figure 7) in the tetragonal unit cell ([111] in the cubic $Fd\bar{3}m$ representation).[17,18] Such a stacking fault is expected to give diffuse scattering streaks along 002 directions of reciprocal space, consistent with those observed in electron diffraction.[8,9,12,48]

Such a feature presumably results from incomplete formation of the γ-Al₂O₃ oxygen sublattice during the transformation process. This 1 nm scale local disorder is unexpected and is distinct from the disorder observed in previous models which have in common a relatively well-ordered oxygen sublattice but disorder on the cation sublattice.[18]

The defect feature highlighted by the local model should be present throughout the structure where bridging of the skeletal layers occurs and atom migration is incomplete. However, there are several degenerate modes of bridging whereby the degree and the direction of the cation translation can vary. By averaging over these degenerate possibilities the local distortions presumably average out resulting in the observed average structure. We demonstrate how the local model can be reconciled with the average structure in Figure

(48) Cowley, J. M. *Acta Crystallogr.* **1953**, *6*, 53−54.
(49) Fleming, S.; Rohl, A. L. *Z. Kristallogr.* **2005**, *220*, 580−584.
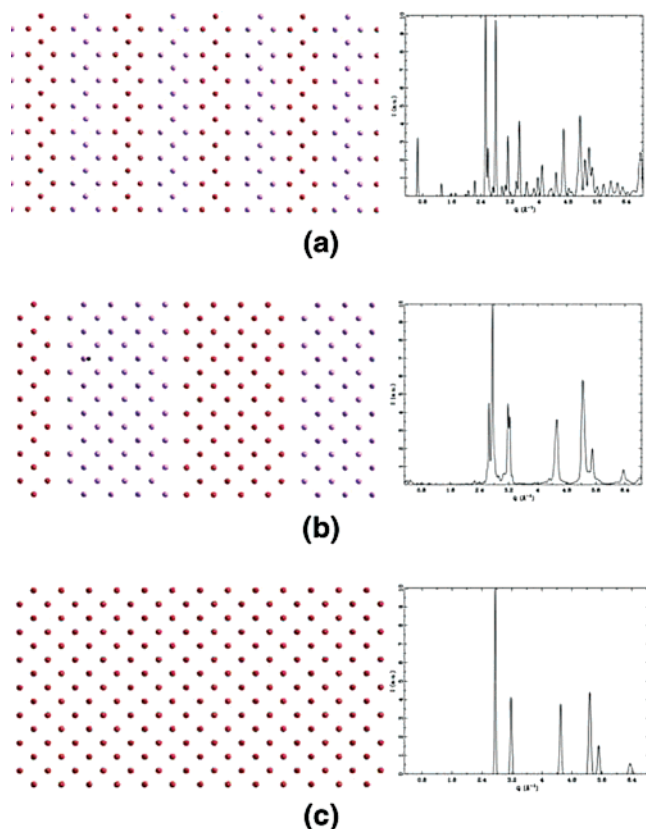
Figure 8. Illustration of (a) the oxygen sublattice with faulted domains equal to half the local model (three atoms), (b) the oxygen sublattice with larger faulted domains in a semi-random aperiodic arrangement, and (c) an unfaulted oxygen sublattice as per the average structural model. The corresponding simulated neutron diffraction patterns, which were generated using GDIS,[49] are shown adjacent. The two different colors for the atoms represent the two offset groups of oxygen atoms. Aluminum has not been included for clarity. Superlattice peaks from the fully ordered local model become less apparent by disordering the fault planes.

8 by comparing supercells of the oxygen sublattice with their neutron diffraction patterns. If the faults are fully ordered, as would be the case for a periodically repeated local model, superlattice peaks appear in the calculated diffraction pattern that are not seen experimentally (Figure 8a). However, by arranging the stacking faults aperiodically the superlattice peaks are suppressed and the observed diffraction pattern is recovered (compare Figure 8b & c). The more randomly the faults are arranged, the more closely the average diffraction pattern is recovered. This rationalizes how a faulted local structure can be reconciled with an apparently unfaulted structure on average.

A further attempt to reconcile the local and average structures was made through refinement of an "artificial" model, which was a $4 \times 1 \times 6$ supercell of the local structure model containing two modes of bridging. This model was termed "artificial" because it does not accurately reproduce the experimental neutron diffraction pattern and, therefore, does not adequately reconcile the local and average structure. However, it does incorporate the stacking fault present in the nanomodel and results in a good fit to the PDF over a wide-range of r with $R_{wp} = 22.8\%$. This was compared to refinements of a $2 \times 1 \times 3$ supercell of the average model under $P1$, which, irrespective of the number of parameters relaxed, the fit did not improve upon that of the c symmetry-based nonspinel model. In fact it resulted in a higher R_{wp} of 34.8%. Both of these models have a large number of parameters (120 and 160 atom coordinates for the local and average supercell models, respectively), and so the results pertaining to these supercells should be treated with caution because they may be over parametrized. However, it is striking that the highly over parametrized model which started from an unfaulted oxygen sublattice could not find a good solution whereas the faulted model was much more successful in fitting the entire range of the PDF.

Conclusions

In summary, we have demonstrated that a previously undetected 1 nm scale modified local structure exists in commercially important γ-Al$_2$O$_3$. The identification of the local structural configuration was made possible by the consideration of diffuse scattering that is incorporated in the PDF. The local structure is explained in terms of stacking defects formed during the creation of γ-Al$_2$O$_3$ from boehmite; the average structure is a superposition of different local degenerate defect structures. The PDF analysis also provides confirmation of the suitability of the recently proposed c symmetry-based nonspinel models for describing the average structure of γ-Al$_2$O$_3$. On the basis of this, it is thought that this misalignment of planes is present throughout the structure of γ-Al$_2$O$_3$ where bridging of the skeletal layers occurs.